Controlling anisotropic dipolar interaction with shielding resonance in a three-dimensional molecular quantum gas

Jun-Ru Li[1,*], William G. Tobias[1], Kyle Matsuda[1], Calder Miller[1], Giacomo Valtolina[1], Luigi De Marco[1], Reuben R. W. Wang[1], Lucas Lassablière[2], Goulven Quéméner[2], John L. Bohn[1], and Jun Ye[1,*]

1. JILA, National Institute of Standards and Technology and Department of Physics, University of Colorado, Boulder, CO, 80309, USA

2. Université Paris-Saclay, CNRS, Laboratoire Aimé Cotton, 91405 Orsay, France

ABSTRACT

Ultracold polar molecules possess long-range, anisotropic, and tunable dipolar interactions, providing unique opportunities to probe novel quantum phenomena[1-4]. However, experimental progress has been hindered by excessive two-body loss, which also limits further cooling via evaporation. Recent work shows the loss can be mitigated by confining molecules in a two-dimensional geometry[5,6]. However, a general approach for tuning molecular interactions in a full three-dimensional (3D) stable system has been lacking. Here, we demonstrate the use of an electric field-induced shielding resonance[6–8] to suppress the reactive loss by a factor of 30 while preserving elastic, long-range dipolar interactions in a bulk gas of ultracold $^{40}K^{87}Rb$ molecules in 3D. The favorable ratio of elastic to inelastic collisions enables direct thermalization, the rate of which depends on the angle between the collisional axis and the dipole orientation controlled by an external electric field. This is a direct manifestation of the anisotropic dipolar interaction. We further achieve dipolar-interaction-mediated evaporative cooling in 3D. This work demonstrates control of a long-lived bulk quantum gas system with tunable long-range interactions, paving the way for the study of collective quantum many-body physics.

INTRODUCTION

The study of atomic quantum gases has benefited from precise control over interactions between their constituents. By tuning the interactions with convenient tools such as external fields[9,10], one can vary the properties of a quantum system and explore its dynamics and phase transitions. Compared to atoms, polar molecules possess large

electric dipole moments and rich energy level structures, making them a unique platform for studying a range of topics such as quantum magnetism[11–14], exotic superfluidity[15–17], precision measurement[18,19] and quantum sensing[20], and quantum information processing[21,22]. However, the realization of tunable-interaction quantum systems based on polar molecules has been impeded by their propensity to undergo rapid collisional losses[23–27], even for molecules without exothermic chemical reactions[25–27]. So far, the loss rate across many species has been found to follow the same universal value[23,28–30], although the responsible mechanisms are still under investigation[31–35].

The recent production of a degenerate Fermi gas of $^{40}K^{87}Rb$ (KRb) molecules led to the surprising discovery of suppressed reaction rates upon entering deep degeneracy[36,37]. Proposed mechanisms for this effect include many-body correlations[38] and higher-order complex-molecule dynamics[39]. This suppression from degeneracy has been observed at zero field. Turning on the dipolar interaction by applying an external electric field $\boldsymbol{E}$ to polarize the molecules led to vastly enhanced losses owing to dipolar attraction[24,40]. Inspired by earlier theory[41,42] and experimental work[43], we recently demonstrated that in a quasi-two-dimensional (quasi-2D) geometry[5], where repulsive dipolar collisions predominate, the two-body loss can be suppressed by more than a factor of 2.

Compared to gases in quasi-2D, a full three-dimensional (3D) gas of polar molecules provides the most general staging platform for studying dipolar gases. Moreover, the long-range nature of the dipolar interaction is more prominent in 3D[44], leading to unique

collective dynamics in bulk dipolar gases[45–49]. Therefore, mitigating the strong two-body loss and tuning the dipolar interactions in a 3D geometry are of great experimental interest. In quasi-2D, we recently demonstrated the suppression of two-body loss by an order of magnitude via resonant shielding arising from modified intermolecular potentials due to dipolar coupling between degenerate collision channels[6].

In this work, we explore the full properties of the resonant collisional shielding in 3D, including the elastic interaction. We show that elastic dipolar collisions are appreciable at the shielding field, thus achieving a long lifetime and controlled dipolar interactions *simultaneously* in 3D. In our optical trap, we first show that the two-body loss rate between reactive molecules in the first excited rotational state is suppressed by a factor of 30 from the background value at the shielding field of $|\boldsymbol{E}_S|$ = 12.72 kV/cm, allowing a lifetime of ~10 s at typical densities of 2.5×10^{11} cm^{-3}. At $|\boldsymbol{E}_S|$, molecules have an induced dipole moment d of –0.08 D and therefore collide elastically via dipolar interactions. We quantitatively characterize these elastic collisions by performing cross-dimensional relaxation experiments after selectively heating along one direction of the molecular gas. An elastic to inelastic collision ratio γ of 12 is measured. We further show that the rate of the relaxation depends on the orientation of the induced dipoles relative to the direction of heating, a signature of the anisotropy of dipolar scattering. As we vary the orientation of the dipoles, we observe a change of the relaxation rate by a factor of 2.5. Leveraging the large γ at $\boldsymbol{E}_S$, we perform efficient evaporative cooling in 3D. Since the shielding

mechanism is predicted to work for a broad class of molecular species[50], our strategy provides a general method for preparing low-entropy molecular samples.

LONG-LIVED GASES OF POLAR MOLECULES IN 3D

KRb suffers from strong reactive two-body losses. While the collision cross section of dipolar elastic collisions increases with d as d^4 (Ref.[51]), reactive losses increase more strongly as d^6 (Ref.[24,40]), preventing the observation of any dynamics related to the elastic dipolar collisions with large dipoles. However, reactive loss of KRb in $|N = 1, m_N = 0\rangle$ is suppressed at certain electric fields. Here, N is the field-dressed rotational quantum number and m_N is its projection onto $\boldsymbol{E}$. The suppression mechanism arises from tuning the collisional channels into degeneracy with $\boldsymbol{E}$, where they are mixed by the resonant dipolar coupling[6–8] . At the center of the resonance, $|\boldsymbol{E}_0| \approx 12.67$ kV/cm, the energy of the collision channel $|1,0\rangle\,|1,0\rangle$ is degenerate with that of $|0,0\rangle\,|2,0\rangle$, where the two kets represent the symmetrized rotational states of the pair of colliding molecules. The two collision channels are mixed by dipolar coupling, the strength of which depends on the spatial separation R between the two molecules. The resultant avoided crossing modifies the energy of the coupled channels and manifests as an effective intermolecular potential (see Supplementary Section 1). In the vicinity of $|\boldsymbol{E}_0|$, for $|\boldsymbol{E}| > |\boldsymbol{E}_0|$, the mixing results in a repulsive energy barrier for $|1,0\rangle\,|1,0\rangle$, preventing the molecules from getting close enough to undergo a chemical reaction. In contrast to the barrier formed by the direct dipolar interaction[5,24,40,42,43], the barrier formed by resonant shielding exists for both

"head-to-tail" and "side-by-side" collisions, shown in Fig. 1**a**, enabling the suppression of two-body loss in 3D. For $|\boldsymbol{E}| < |\boldsymbol{E}_0|$, the effective potential is mainly attractive, resulting in enhanced loss (Fig. 1**b**).

We measure the shielding effect by monitoring the decay rate of the average molecular density n at different $|\boldsymbol{E}|$. Molecular gases are prepared following the procedure described in Ref.[36]. Briefly, we start with a degenerate mixture of ^{40}K and ^{87}Rb in an optical dipole trap (ODT). Molecules in $|0,0\rangle$ are created via magnetoassociation around 546.62 G followed by stimulated Raman adiabatic passage (STIRAP) at an electric field of $\boldsymbol{E}_{\mathrm{STIRAP}}$ = 4.5 kV/cm. A microwave Rabi π–pulse then transfers the molecules to $|1,0\rangle$ before $\boldsymbol{E}$ is ramped from $\boldsymbol{E}_{\mathrm{STIRAP}}$ to its target value in 60 ms. We typically have 1.5×10^4 molecules in $|1,0\rangle$ at T = 300 nK with a density of 2.5×10^{11} cm^{-3} after the field ramp. After a variable hold time t, $\boldsymbol{E}$ is ramped back to $\boldsymbol{E}_{\mathrm{STIRAP}}$ where the molecules are transferred back to $|0,0\rangle$, dissociated to the Feshbach state, and imaged after time-of-flight expansion. The ODT has trapping frequencies of $(\omega_x, \omega_y, \omega_z) = 2\pi \times (45, 250, 40)$ Hz for $|1,0\rangle$ at $\boldsymbol{E}_{\mathrm{STIRAP}}$, with weak dependence on $\boldsymbol{E}$ (Methods). In contrast to Ref.[5,6] where only the lowest harmonic level along the tightly confined direction is dominantly populated, here we have $k_B T \gg \hbar\omega_i$ for all three directions, fulfilling the criterion of a 3D geometry ($\hbar$ is the reduced Planck constant and k_B is the Boltzmann constant).

The reactive two-body loss rate β is extracted by fitting the decay of n with $\dot{n} = -\beta\, n^2 - (3n/2T)\dot{T}$, where the first term is the reactive loss and the second term accounts for the

density change due to "anti-evaporation"[24]. The resonant shielding effect is manifested as two sharp features in β around $|\boldsymbol{E}|$ = 11.5 kV/cm and 12.5 kV/cm, as shown in Fig. 2**a**. The two resonant features correspond to the coupled open channels $|1,0\rangle\,|1,0\rangle \rightarrow |0,0\rangle\,|2,\pm1\rangle$ and $|1,0\rangle\,|1,0\rangle \rightarrow |0,0\rangle\,|2,0\rangle$, respectively. The width of each feature is around 100 V/cm, determined by the differential dipole moments of the involved rotational states and the strength of the dipolar coupling (see Supplementary Section 1). Near the resonances, β varies by 3 orders of magnitude within a change of $|\boldsymbol{E}|$ of 0.25 kV/cm. Two decay curves exemplifying this contrast are displayed in Fig. 2**b** and Fig. 2**c**. At $|\boldsymbol{E}_S|$= 12.72 kV/cm, we observe long-lived (~10s) molecular gases in 3D (Fig. 2**b**). When $|\boldsymbol{E}|$ is tuned far from the resonances, β increases with the increasing d, similar to KRb in $|0,0\rangle$ (Ref.[24]). At $|\boldsymbol{E}|$ = 4.5 kV/cm, where the molecules have a similar dipole moment as at $|\boldsymbol{E}_S|$, the lifetime is much shorter (~1s), highlighting the prominent effect of resonant dipolar shielding of the two-body loss.

ANISOTROPIC DIPOLAR THERMALIZATION

This long-lived molecular gas offers a practical platform to explore the effect of dipolar elastic collisions between reactive molecules. The elastic collisions have a rate of $n\sigma_{el}v$, where σ_{el} is the elastic cross section and v is the ensemble-averaged relative collisional velocity of two molecules (see Methods). In general, the cross section for dipolar collisions depends on the relative kinetic energy of the two colliders. However, in the ultracold regime, σ_{el} approaches a universal value $\sigma_{el} = (32\pi/15)\, a_d^2$ for indistinguishable fermionic scatterers[51], which is independent of the collision energy. Here, $a_d = (m/2)d^2/(4\pi\varepsilon_0\hbar^2)$ and

m is the mass of the molecule. Near $|\boldsymbol{E}_S|$, the resonant dipolar coupling modifies the intermolecular potential and hence could also affect the properties of the elastic collisions. However, the low-energy collisions are to a large extent determined by the long-range tail of the intermolecular potential[51]. This is not strongly affected by the shielding potential barrier, which occurs at a Van der Waals length scale $\sim 10^2$ Bohr radius. We therefore expect that the universal result for the dipolar cross section is valid at $\boldsymbol{E}_S$, giving $\sigma_{el} = 2.8\times10^{-12}$ cm^2, with $d \approx -0.08$ D for $|1,0\rangle$ at $\boldsymbol{E}_S$. Calculations[7] predict $\gamma = 17.8$ for a molecular gas of $T = 330$ nK at the shielding field (Fig. 1**c**), large enough for thermalization within the ensemble lifetime.

We experimentally demonstrate and characterize the dipolar elastic collisions through cross-dimensional thermalization, with a geometry shown in Fig. 3**c**. The molecular gas is heated along the more tightly confining y-direction. Elastic collisions redistribute the excess kinetic energy from $\boldsymbol{y}$ to $\boldsymbol{x}$ and $\boldsymbol{z}$. The rate Γ_{th} of this relaxation process is proportional to the elastic cross collision rate as

$$\Gamma_{th} = \frac{n\sigma_{el}v}{N_{coll}}. \qquad (1)$$

Here the factor N_{coll} is physically interpreted as the number of collisions required to thermalize. N_{coll} has been calculated to be 2.7 and 4.1 for s-wave[52] and p-wave[53] collisions, respectively. For dipolar elastic collisions, theoretical calculations[54] and experiments with magnetic atoms[55,56] have shown that N_{coll} depends on the angle θ between the dipole and the direction of heating y. This is a direct result of the anisotropic dipolar collisions.

We observe the anisotropic elastic relaxation process using the following experimental procedure. The molecules are initially prepared in thermal equilibrium in $|1,0\rangle$ at $|\boldsymbol{E}_S| =$ 12.72 kV/cm with $\theta = 0^\circ$. The field is then rotated to the target angle θ in 60 ms. Next, a temperature imbalance between the trap axes is introduced by parametrically heating the molecular cloud along ***y*** for 50–100 ms (inset of Fig. 3**c**), which is much shorter than the time scale of thermalization. We create an initial condition of $T_y \approx 2.5\ T_x$. The relaxation process is observed by monitoring the time evolution of T_y and T_x as the sample thermalizes in the trap.

As the gas equilibrates, the temperatures approach each other. The temperature evolution for $\theta = 45^\circ$ and $\theta = 90^\circ$ is shown in Fig. 3**a** and 3**b**, respectively. A clear difference in the thermalization rates for the two orientation angles is observed. We quantitatively study the relaxation by fitting the trajectories of T_x, T_y, and n with a set of coupled differential equations (Methods). The equations capture two physical processes contributing to the temperature change: the elastic dipolar collisions associated with N_{coll}, and the reactive loss, associated with the loss coefficient K_L, which preferentially removes two colliders with high relative kinetic energy[24]. Here, K_L is related to β as $K_L = (1/3)\ \beta/T$ for a thermally-equilibrated gas at temperature T.

For each θ, we extract N_{coll} and K_L from the fits. We observe a clear angular dependence of the number of collisions required for thermalization, summarized in Fig. 3**c**. At 45°, only

$1.6^{+0.2}_{-0.1}$ collisions are required for thermalization while $4.1^{+0.9}_{-0.6}$ collisions are required for θ = 90°. In the limit of small parametric excitation and using the scattering cross section of point dipoles, N_{coll} can be calculated analytically within the Enskog formalism. Adopting the computational techniques used in Ref.[57] permits the concise analytic expression:

$$N_{coll}(\theta) = \frac{56}{33 - 17\cos 4\theta} \qquad (2)$$

for a gas heated along ***y***, and rethermalization measured along ***x***. More details of the derivation are provided in the Supplementary Section 2. Equation (2) (gray solid curve, Fig. 3**c**) describes the measured angular dependence quite well, despite the approximations above. From the measured K_L, we calculate $\gamma = \sigma_{el}\, v/(3K_L T)$ as high as 12(1), confirming the dominant role of the elastic collisions in the observed temperature evolution.

EVAPORATIVE COOLING OF MOLECULES IN 3D

A large γ enables direct evaporative cooling of KRb in 3D. Moreover, the Wigner threshold law[23,58] suggests γ will increase further at lower temperatures for fermionic molecules as $\gamma \sim 1/\sqrt{T}$, which facilitates the evaporative cooling processes. We perform evaporation by lowering the depth of the optical trap at $\theta = 0°$. During evaporation, we observe that the *x* and *y* directions remain in equilibrium and the temperature *T* drops along with the number of molecules N_{KRb} remaining in the trap. Efficient evaporation, where the phase-space density (PSD) increases over the trajectory, requires the slope $S_{evap} = \partial \ln N_{KRb} / \partial \ln T$ to be smaller than 3 in 3D. We measure S_{evap} = 1.84(9), significantly below this threshold (Fig. 4). Over the trajectory, the PSD increases from 0.014(1) to

0.06(2), corresponding to a decrease of T/T_F from 2.3(1) to 1.4(2) (T_F is the Fermi temperature). Compared with the procedure in Ref.[36] that produced a degenerate Fermi gas at $T/T_F = 0.3$ with $N_{KRb} = 2.5\times10^4$, the present approach requires preparing molecules in $|1,0\rangle$ at $|\boldsymbol{E}_S|$. This requires a ramp of the electric field that causes molecular loss and heating, limiting the highest PSD achieved in this work. Future technical improvements, such as direct creation of molecules at $|\boldsymbol{E}_S|$, will enable evaporation of molecular gases to deep quantum degeneracy.

CONCLUSIONS

Employing an electric-field tuned shielding resonance, we have demonstrated anisotropic thermalization via dipolar elastic collisions and performed efficient evaporative cooling of reactive polar molecules in 3D. The two-body loss is greatly suppressed by resonant dipolar shielding, giving a ratio of elastic to reactive collision rates as high as 12. Our work highlights a general approach for controlling the interaction properties of polar molecules in 3D. The same mechanism has been predicted to be effective for other molecules, for which even higher ratios [50] and even more efficient evaporation may be achievable. Our findings demonstrate a promising strategy for producing low-entropy molecular gases in bulk systems and open the door for a broad range of applications in molecule-based quantum platforms.

Note: During the preparation of this manuscript we became aware of a recent work (Ref.[59]) reporting microwave shielding in a molecular tweezer.

METHODS

Thermalization Model

We fit the temperature and density evolution with a set of differential equations[24]:

$$\dot{n} = -K_{\mathrm{L}}(T_{\mathrm{y}} + 2T_{\mathrm{x}})n^2 + \frac{n}{2T_{\mathrm{y}}}\dot{T}_{\mathrm{y}} + \frac{n}{T_{\mathrm{x}}}\dot{T}_{\mathrm{x}}$$

$$\dot{T}_{\mathrm{y}} = \frac{n}{4}K_{\mathrm{L}}(-T_{\mathrm{y}} + 2T_{\mathrm{x}})T_{\mathrm{y}} - \frac{2\Gamma_{\mathrm{th}}}{3}(T_{\mathrm{y}} - T_{\mathrm{x}}) + c_{\mathrm{y}}$$

$$\dot{T}_{\mathrm{x}} = \frac{n}{4}K_{\mathrm{L}}T_{\mathrm{y}}T_{\mathrm{x}} + \frac{\Gamma_{\mathrm{th}}}{3}(T_{\mathrm{y}} - T_{\mathrm{x}}) + c_{\mathrm{x}}\,. \qquad (3)$$

Γ_{th} is defined in equation (1) with $v = \sqrt{16k_B(T_y + 2T_x)/(3\pi m)}$. K_{L} describes the two-body loss and c_{y} and c_{x} are background heating rates. The model captures the two main contributions to the observed temperature evolution: the elastic dipolar collisions described by the term proportional to Γ_{th}, and the effects on the temperature from the reactive loss described by the first term related to K_{L}.

The model has two assumptions for simplicity. First, we assume a similar reaction coefficient K_{L} for molecules colliding along different directions with respect to the dipole, which is valid in the vicinity of $|\boldsymbol{E}_{\mathrm{S}}|$[6]. Second, the temperatures of the two unmodulated directions *x* and *z* remain identical during the thermalization process. Systematic error introduced by this assumption is maximized at the angle of 45° where the thermalization speed between ***y***, ***x*** and ***y***, ***z*** differs by the most. Since the thermalization between ***y***, ***z*** is much slower, adopting this assumption leads us to underestimate the thermalization rate around 45°.

Data Analysis

For each θ, we image the molecules at several hold times between 0.05 and 10 s, at several times-of-flight between 1.5 and 8.2 ms, and with and without parametric heating. To minimize the systematic effects from slow drift in experimental conditions, we randomize the order in which the data is taken. For each hold time and heating condition, we fit the temperatures T_x and T_y and average density n, assuming free expansion of the cloud. Estimated values and their covariance matrix are obtained via bootstrapping. We fit the temperature and density decay curves to equation (3), treating K_L, N_{coll}, c_x, c_y, and the initial temperatures and densities as fit parameters. To estimate confidence intervals on the fit parameters, we generate 100 synthetic datasets by independently drawing new temperatures and densities at each time point from a multivariate normal distribution. The reported parameters and confidence intervals represent the median and the intervals containing 68% of the trials. This approach lets us examine correlations between the different fit parameters. An example fit is shown in Extended Data Fig.1**a** for $\theta = 45^\circ$. The fit yields $N_{coll} = 1.57(14)$, $K_L = 3.8(3) \times 10^{-7}$ cm^{3}s^{-1}K^{-1}.

Extended Data Fig. 1**b** shows the fitted result for 100 synthetic datasets. The small correlation of -0.26 between N_{coll} and K_L indicates that the fitting distinguishes between the thermalization and two-body loss well.

Extended Data Fig. 1**c** shows the extracted loss rate K_L vs. θ. Though the measured K_L seems to be anti-correlated with N_{coll}, we find that the observed variation of K_L is not

drastic enough to cause a significant change to the extracted N_{coll}. This weak modulation of K_L could be caused by daily technical drifts on the electric field strength or residual field gradient, or contributions of the higher partial wave in the two-body collisions which may cause a higher K_L around $\theta \approx 54^\circ$ where the shielding barrier is weak.

Temperature Measurement

Temperatures are measured by fitting the Gaussian width of the cloud after time-of-flight expansion. To image the molecules, the electric field $\boldsymbol{E}$ is ramped from $\boldsymbol{E}_S$ back to $\boldsymbol{E}_{STIRAP}$ after the hold time. The molecules are then transferred to $|0,0\rangle$ and dissociated for imaging. The changes in the bias field and molecular rotational state result in changes to the molecular polarizability and, consequently, the trapping potential. To obtain accurate temperatures of the molecular gas during the thermalization process, we correct for such systematics as detailed below.

Transferring from $|1,0\rangle$ to $|0,0\rangle$ while the molecules are still in the trap causes an instantaneous change of the trapping potential and thus breathing of the cloud, which would introduce errors in the measured temperatures. We avoid this issue by performing the rotational state transfer and STIRAP during time-of-flight.

The ramp down of the electric field from the measurement condition to $\boldsymbol{E}_{STIRAP}$ modifies the trapping potential due to the polarizability change of $|1,0\rangle$ molecules with the bias field. Since this ramp is adiabatic with respect to the single particle trapping periods along all the spatial direction, the resultant adiabatic compression/decompression modifies the

molecular temperature. We calculate the actual temperatures T_i during the thermalization process from the measured temperature T_i^m by

$$T_i = \left(\frac{\omega_i^S}{\omega_i^{STIRAP}} \right) T_i^m . \quad (4)$$

Here, ω_i^S and ω_i^{STIRAP} are the trapping frequencies along *i* at $\boldsymbol{E}_S$ and $\boldsymbol{E}_{STIRAP}$, respectively. The trapping frequencies are calibrated by measuring the parametric heating resonances at each theta. The temperatures reported in the manuscript are T_i.

Data Availability

The data that support the findings of this study are available from the corresponding author upon reasonable request. Source data are provided with this paper.

REFERENCES

1. Ni, K.-K. *et al.* A High Phase-Space-Density Gas of Polar Molecules. *Science* **322**, 231–235 (2008).
2. Quéméner, G. & Julienne, P. S. Ultracold Molecules under Control! *Chem. Rev.* **112**, 4949–5011 (2012).
3. Carr, L. D., DeMille, D., Krems, R. V & Ye, J. Cold and ultracold molecules: science, technology and applications. *New J. Phys.* **11**, 55049 (2009).
4. Bohn, J. L., Rey, A. M. & Ye, J. Cold molecules: Progress in quantum engineering of chemistry and quantum matter. *Science* **357**, 1002–1010 (2017).
5. Valtolina, G. *et al.* Dipolar evaporation of reactive molecules to below the Fermi temperature. *Nature* **588**, 239–243 (2020).
6. Matsuda, K. *et al.* Resonant collisional shielding of reactive molecules using

electric fields. *Science* **370**, 1324–1327 (2020).

7. Wang, G. & Quéméner, G. Tuning ultracold collisions of excited rotational dipolar molecules. *New J. Phys.* **17**, 35015 (2015).
8. Avdeenkov, A. V, Kajita, M. & Bohn, J. L. Suppression of inelastic collisions of polar $^1\Sigma$ state molecules in an electrostatic field. *Phys. Rev. A* **73**, 22707 (2006).
9. Chin, C., Grimm, R., Julienne, P. & Tiesinga, E. Feshbach resonances in ultracold gases. *Rev. Mod. Phys.* **82**, 1225–1286 (2010).
10. Saffman, M., Walker, T. G. & Mølmer, K. Quantum information with Rydberg atoms. *Rev. Mod. Phys.* **82**, 2313–2363 (2010).
11. Gorshkov, A. V *et al.* Quantum magnetism with polar alkali-metal dimers. *Phys. Rev. A* **84**, 33619 (2011).
12. Peter, D., Müller, S., Wessel, S. & Büchler, H. P. Anomalous Behavior of Spin Systems with Dipolar Interactions. *Phys. Rev. Lett.* **109**, 25303 (2012).
13. Yan, B. *et al.* Observation of dipolar spin-exchange interactions with lattice-confined polar molecules. *Nature* **501**, 521–525 (2013).
14. Yao, N. Y., Zaletel, M. P., Stamper-Kurn, D. M. & Vishwanath, A. A quantum dipolar spin liquid. *Nat. Phys.* **14**, 405–410 (2018).
15. Cooper, N. R. & Shlyapnikov, G. V. Stable Topological Superfluid Phase of Ultracold Polar Fermionic Molecules. *Phys. Rev. Lett.* **103**, 155302 (2009).
16. Pikovski, A., Klawunn, M., Shlyapnikov, G. V & Santos, L. Interlayer Superfluidity in Bilayer Systems of Fermionic Polar Molecules. *Phys. Rev. Lett.* **105**, 215302 (2010).

17. Baranov, M. A., Mar'enko, M. S., Rychkov, V. S. & Shlyapnikov, G. V. Superfluid pairing in a polarized dipolar Fermi gas. *Phys. Rev. A* **66**, 13606 (2002).

18. Andreev, V. *et al.* Improved limit on the electric dipole moment of the electron. *Nature* **562**, 355–360 (2018).

19. Cairncross, W. B. & Ye, J. Atoms and molecules in the search for time-reversal symmetry violation. *Nat. Rev. Phys.* **1**, 510–521 (2019).

20. Bilitewski, T. *et al.* Dynamical generation of spin squeezing in ultra-cold dipolar molecules. Preprint at https://arxiv.org/abs/2011.08202 (2020).

21. André, A. *et al.* A coherent all-electrical interface between polar molecules and mesoscopic superconducting resonators. *Nat. Phys.* **2**, 636–642 (2006).

22. Ni, K.-K., Rosenband, T. & Grimes, D. D. Dipolar exchange quantum logic gate with polar molecules. *Chem. Sci.* **9**, 6830–6838 (2018).

23. Ospelkaus, S. *et al.* Quantum-State Controlled Chemical Reactions of Ultracold Potassium-Rubidium Molecules. *Science* **327**, 853–857 (2010).

24. Ni, K.-K. *et al.* Dipolar collisions of polar molecules in the quantum regime. *Nature* **464**, 1324–1328 (2010).

25. Takekoshi, T. *et al.* Ultracold Dense Samples of Dipolar RbCs Molecules in the Rovibrational and Hyperfine Ground State. *Phys. Rev. Lett.* **113**, 205301 (2014).

26. Guo, M. *et al.* Creation of an Ultracold Gas of Ground-State Dipolar $^{23}Na^{87}Rb$ Molecules. *Phys. Rev. Lett.* **116**, 205303 (2016).

27. Park, J. W., Will, S. A. & Zwierlein, M. W. Ultracold Dipolar Gas of Fermionic $^{23}Na^{40}K$ Molecules in Their Absolute Ground State. *Phys. Rev. Lett.* **114**, 205302

(2015).

28. Guo, M. *et al.* Dipolar Collisions of Ultracold Ground-State Bosonic Molecules. *Phys. Rev. X* **8**, 41044 (2018).

29. Ye, X., Guo, M., González-Martínez, M. L., Quéméner, G. & Wang, D. Collisions of ultracold $^{23}Na^{87}Rb$ molecules with controlled chemical reactivities. *Sci. Adv.* **4**, (2018).

30. Gregory, P. D. *et al.* Sticky collisions of ultracold RbCs molecules. *Nat. Commun.* **10**, 3104 (2019).

31. Mayle, M., Quéméner, G., Ruzic, B. P. & Bohn, J. L. Scattering of ultracold molecules in the highly resonant regime. *Phys. Rev. A* **87**, 12709 (2013).

32. Christianen, A., Zwierlein, M. W., Groenenboom, G. C. & Karman, T. Photoinduced Two-Body Loss of Ultracold Molecules. *Phys. Rev. Lett.* **123**, 123402 (2019).

33. Gregory, P. D., Blackmore, J. A., Bromley, S. L. & Cornish, S. L. Loss of Ultracold $^{87}Rb^{133}Cs$ Molecules via Optical Excitation of Long-Lived Two-Body Collision Complexes. *Phys. Rev. Lett.* **124**, 163402 (2020).

34. Liu, Y. *et al.* Photo-excitation of long-lived transient intermediates in ultracold reactions. *Nat. Phys.* **16**, 1132–1136 (2020).

35. Hu, M.-G. *et al.* Direct observation of bimolecular reactions of ultracold KRb molecules. *Science* **366**, 1111–1115 (2019).

36. De Marco, L. *et al.* A degenerate Fermi gas of polar molecules. *Science* **363**, 853–856 (2019).

37. Tobias, W. G. *et al.* Thermalization and Sub-Poissonian Density Fluctuations in a Degenerate Molecular Fermi Gas. *Phys. Rev. Lett.* **124**, 33401 (2020).

38. He, M., Lv, C., Lin, H.-Q. & Zhou, Q. Universal relations for ultracold reactive molecules. *Sci. Adv.* **6**, (2020).

39. He, P., Bilitewski, T., Greene, C. H. & Rey, A. M. Exploring chemical reactions in a quantum degenerate gas of polar molecules via complex formation. *Phys. Rev. A* **102**, 63322 (2020).

40. Quéméner, G. & Bohn, J. L. Strong dependence of ultracold chemical rates on electric dipole moments. *Phys. Rev. A* **81**, 22702 (2010).

41. Micheli, A. *et al.* Universal Rates for Reactive Ultracold Polar Molecules in Reduced Dimensions. *Phys. Rev. Lett.* **105**, 73202 (2010).

42. Quéméner, G. & Bohn, J. L. Dynamics of ultracold molecules in confined geometry and electric field. *Phys. Rev. A* **83**, 12705 (2011).

43. de Miranda, M. H. G. *et al.* Controlling the quantum stereodynamics of ultracold bimolecular reactions. *Nat. Phys.* **7**, 502–507 (2011).

44. Lahaye, T., Menotti, C., Santos, L., Lewenstein, M. & Pfau, T. The physics of dipolar bosonic quantum gases. *Reports Prog. Phys.* **72**, 126401 (2009).

45. Baranov, M. A., Dalmonte, M., Pupillo, G. & Zoller, P. Condensed Matter Theory of Dipolar Quantum Gases. *Chem. Rev.* **112**, 5012–5061 (2012).

46. Ronen, S. & Bohn, J. L. Zero sound in dipolar Fermi gases. *Phys. Rev. A* **81**, 33601 (2010).

47. Fregoso, B. M. & Fradkin, E. Ferronematic Ground State of the Dilute Dipolar

Fermi Gas. *Phys. Rev. Lett.* **103**, 205301 (2009).

48. Wilson, R. M., Ronen, S. & Bohn, J. L. Critical Superfluid Velocity in a Trapped Dipolar Gas. *Phys. Rev. Lett.* **104**, 94501 (2010).

49. Liu, B., Li, X., Yin, L. & Liu, W. V. Weyl Superfluidity in a Three-Dimensional Dipolar Fermi Gas. *Phys. Rev. Lett.* **114**, 45302 (2015).

50. González-Martínez, M. L., Bohn, J. L. & Quéméner, G. Adimensional theory of shielding in ultracold collisions of dipolar rotors. *Phys. Rev. A* **96**, 32718 (2017).

51. Bohn, J. L., Cavagnero, M. & Ticknor, C. Quasi-universal dipolar scattering in cold and ultracold gases. *New J. Phys.* **11**, 55039 (2009).

52. Monroe, C. R., Cornell, E. A., Sackett, C. A., Myatt, C. J. & Wieman, C. E. Measurement of Cs-Cs elastic scattering at T=30 μK. *Phys. Rev. Lett.* **70**, 414–417 (1993).

53. DeMarco, B., Bohn, J. L., Burke, J. P., Holland, M. & Jin, D. S. Measurement of *p*-Wave Threshold Law Using Evaporatively Cooled Fermionic Atoms. *Phys. Rev. Lett.* **82**, 4208–4211 (1999).

54. Bohn, J. L. & Jin, D. S. Differential scattering and rethermalization in ultracold dipolar gases. *Phys. Rev. A* **89**, 22702 (2014).

55. Aikawa, K. *et al.* Anisotropic Relaxation Dynamics in a Dipolar Fermi Gas Driven Out of Equilibrium. *Phys. Rev. Lett.* **113**, 263201 (2014).

56. Tang, Y., Sykes, A., Burdick, N. Q., Bohn, J. L. & Lev, B. L. *s*-wave scattering lengths of the strongly dipolar bosons ^{162}Dy and ^{164}Dy. *Phys. Rev. A* **92**, 22703 (2015).

57. Wang, R. R. W., Sykes, A. G. & Bohn, J. L. Linear response of a periodically driven thermal dipolar gas. *Phys. Rev. A* **102**, 33336 (2020).

58. Sadeghpour, H. R. *et al.* Collisions near threshold in atomic and molecular physics. *J. Phys. B At. Mol. Opt. Phys.* **33**, R93--R140 (2000).

59. Anderegg, L. *et al.* Observation of Microwave Shielding of Ultracold Molecules. Preprint at https://arxiv.org/abs/2102.04365 (2021).

ACKNOWLEDGEMENTS

We acknowledge funding from ARO-MURI, AFOSR-MURI, DARPA DRINQS, NSFQLCI OMA–2016244, NIST, and NSF grant 1806971. L. L. and G. Q. acknowledge funding from the FEW2MANY-SHIELD Project No. ANR-17-CE30-0015 from Agence Nationale de la Recherche. We thank Lee R. Liu for reading the manuscript.

AUTHOR CONTRIBUTIONS

J.-R. L., W. G. T., K. M., C. M., G. V., L. D. M., and J. Y. contributed to the experimental measurements. L. L. and G. Q. calculated the effective intermolecular potential. R. R. W. W. and J. L. B. calculated the anisotropic thermalization rate. All authors discussed the results, contributed to the data analysis, and worked on the manuscript.

COMPETING INTERESTS The authors declare no competing interests.

MATERIALS & CORRESPONDENCE Correspondence and material requests should be addressed to Jun-Ru Li (junru.li@colorado.edu) and Jun Ye (Ye@jila.colorado.edu).

AUTHOR INFORMATION

Giacomo Valtolina:

Present address: Fritz-Haber-Institut der Max-Planck-Gesellschaft, Faradayweg 4-6, 14195Berlin, Germany

ADDITIONAL INFORMATION

Supplementary Information section 1, 2 including Fig.S1 are available for this paper.

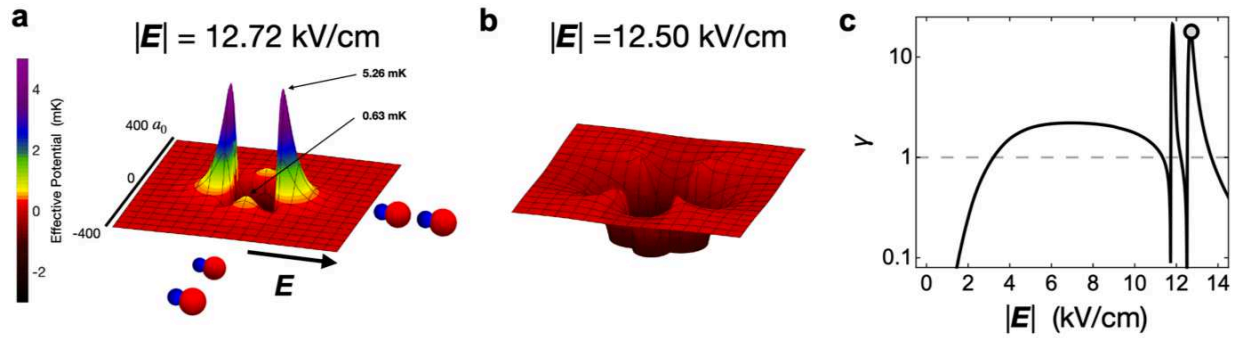

Figure 1. Effective intermolecular potential and molecular scattering near the shielding resonance. a and **b**, Calculated effective intermolecular potential for KRb in $|1,0\rangle$ at $|\boldsymbol{E}|$ = 12.72 kV/cm and $|\boldsymbol{E}|$ = 12.50 kV/cm respectively (see Supplementary Section 1). The resonant dipolar coupling mixes two degenerate collisional channels. The strong mixing between the channels modifies the intermolecular potential and results in either suppression or enhancement of the two-body loss rate depending on $|\boldsymbol{E}|$. a_0 is the Bohr radius. **c**, Calculated ratio γ of the elastic rate to reactive rate for KRb in $|1,0\rangle$ at T = 330 nK[7]. Our experiment is carried out at $|\boldsymbol{E}_S|$ = 12.72 kV/cm (indicated by the gray point) where γ of 17.8 is calculated. The gray dashed line indicates γ = 1.

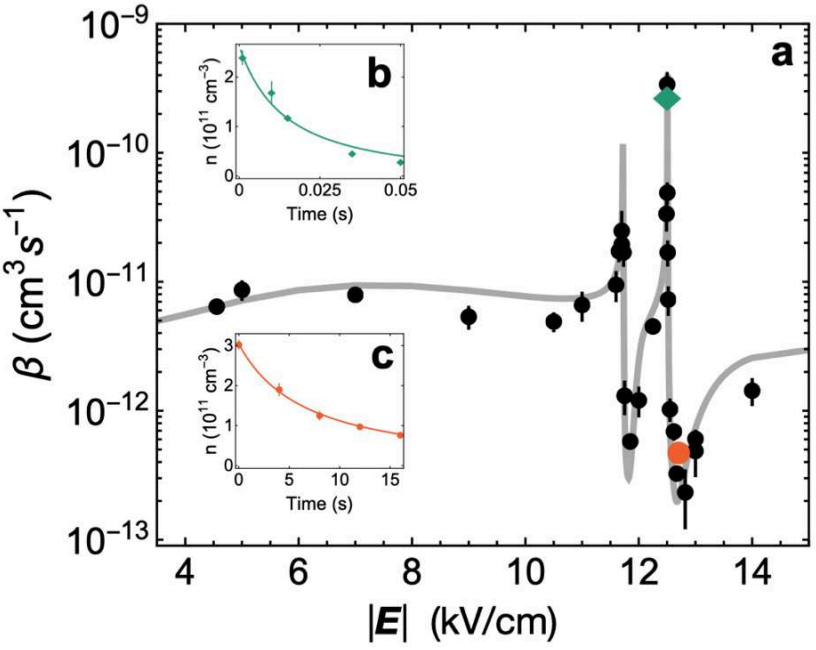

Figure 2. Resonant shielding of the reactive loss in 3D. a, Measured two-body loss rate versus electric field strength. The solid line is the theoretical calculation for the experimental condition T = 330 nK with no free parameters. The green diamond and orange circle identify the fields for which decay curves are plotted in insets **b** and **c**, respectively. Insets: Molecule loss measurements at |***E***| = 12.50 kV/cm (**b**) and 12.72 kV/cm (**c**) where the loss is enhanced and suppressed respectively. Solid lines are fits to the two-body loss rate equation.

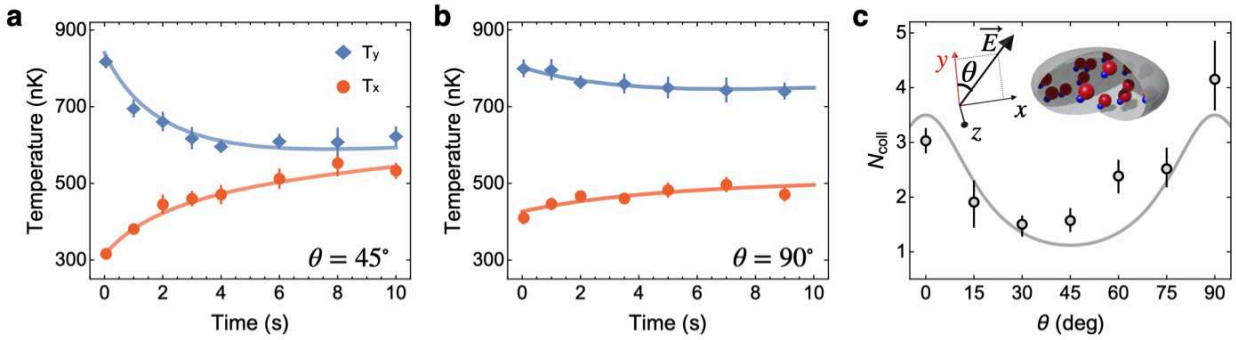

Figure 3. Anisotropic cross-dimensional thermalization of molecules via dipolar elastic collisions. a and **b**, Time evolution of the temperature for $\theta = 45^\circ$ and $\theta = 90^\circ$ after parametric heating along ***y***. The solid lines are fits to our model (Methods). The thermalization is faster at $\theta = 45^\circ$. T_z is not directly measured and is assumed to be the same as T_x during the entire process. Error bars are 1 SE. **c**, Angle-dependent number of collisions required for the rethermalization of dipolar Fermi gases. N_{coll} is extracted by fitting the time evolution of the temperature (Methods). The gray solid line represents the calculated analytical expression, equation (2). Inset: Geometry of the experiment. Molecules are polarized with a bias field ***E*** whose orientation angle θ is varied between 0° and 90° within the *x*–*y* plane. The molecular gases are heated parametrically along the *y* direction to create an initial condition of $T_y \approx 2.5\ T_x$, $T_x = T_z$.

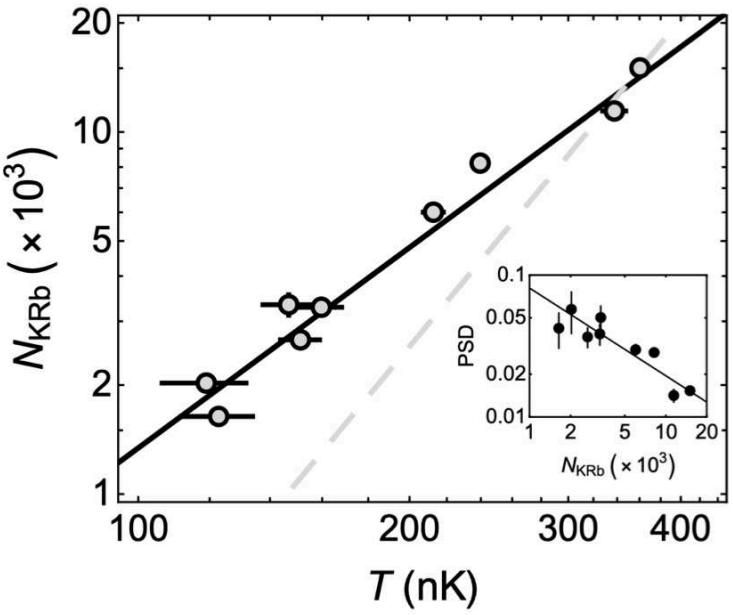

Figure 4. Efficient evaporative cooling of reactive polar molecules in 3D. Evolution of N_{KRb} and T at different stages of the evaporation trajectory at $|\boldsymbol{E}|$ and with $\theta = 0^{\circ}$. The power-law fits (black line) yields S_{evap} = 1.84(9), indicating efficient evaporation. The dashed line represents a constant PSD. Error bars are 1 SE. Inset: PSD $(N_{KRb}(\hbar\bar{\omega}/k_B T)^3)$ versus N_{KRb} during evaporation, displaying a clear gain. Here, $\bar{\omega}$ is the geometric mean of the trapping frequencies. $\bar{\omega}$

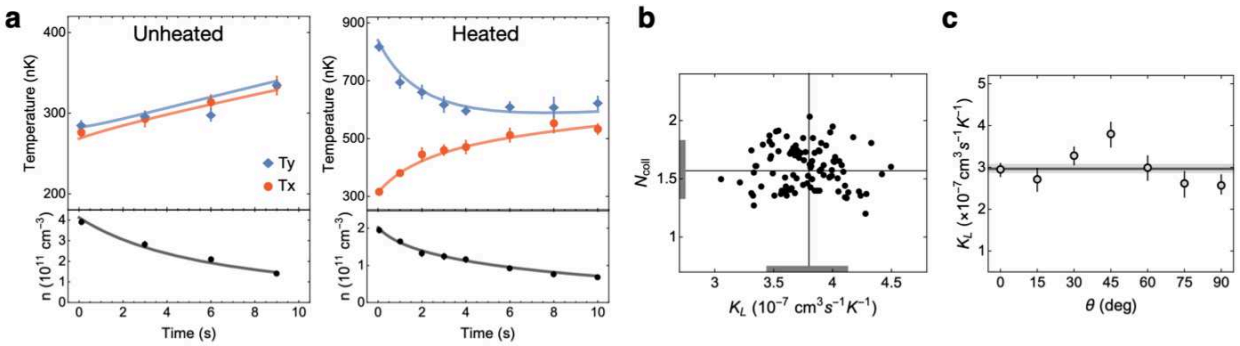

Extended Data Figure 1. Fitting experimental data with the model. The figure shows the fit results for $\theta = 45^\circ$. **a**, Fitting of the unheated and heated data. **b**, Fitted K_L and N_{coll} for 100 synthetic datasets. We extract a correlation of -0.26 between the two fitted parameters, indicating that the fitting can distinguish between two-body loss and thermalization. The black solid lines are the median of all the fitted results from the synthetic datasets for N_{coll} and K_L, while the gray lines on the axis represent 68% confidence interval of the fitted results. This median and 68% confidence are reported in the main text. **c**, Extracted loss coefficient K_L versus θ. The line and shaded region indicate the mean value of K_L and its standard error.

Supplementary Information for Controlling anisotropic dipolar interaction with shielding resonance in a three-dimensional molecular quantum gas

Jun-Ru Li,[1] William G. Tobias,[1] Kyle Matsuda,[1] Calder Miller,[1] Giacomo Valtolina,[1] Luigi De Marco,[1] Reuben R. W. Wang,[1] Lucas Lassablière,[2] Goulven Quéméner,[2] John L. Bohn,[1] and Jun Ye[1]

[1] *JILA, National Institute of Standards and Technology and Department of Physics, University of Colorado, Boulder, CO, 80309, USA*

[2] *Université Paris-Saclay, CNRS, Laboratoire Aimé Cotton, 91405 Orsay, France.*

SIMPLIFIED THEORY OF RESONANT SHIELDING

The section presents a simplified theory to demonstrate how resonant dipolar coupling modifies the intermolecular potential and gives rise to the suppressed two-body loss. Discussions in this section implement several assumptions that are not exact, but nevertheless capture the essential ingredients required for the resonant shielding mechanism. More complete and detailed discussions can be found in Ref. [1, 2].

The total wavefuction of two colliding polar molecules can be written as

$$|L, m_{\mathrm{L}}\rangle|N, m_{\mathrm{N}}\rangle|N', m_{\mathrm{N}'}\rangle, \tag{S1}$$

where L and m_L is the orbital angular momentum of the relative motion and m_L is its projection onto a quantization axis. $N, N', m_N, m_{N'}$ are each molecule's rotational quantum numbers and their projection onto the polarization axis set by an external electric field. With non-zero electric field, $|N, m_{\mathrm{N}}\rangle, |N', m_{\mathrm{N}'}\rangle$ refer to the properly dressed state.

Dipolar interaction couples different collisional channels by allowing the exchange of the internal rotations of the two colliders, and exchange of the angular momentum between the internal rotation and the orbit. Taking the resonant shielding at $|\boldsymbol{E}_{\mathrm{s}}| = 12.72$ kV/cm for example, the relevant term of this dipolar coupling reads

$$\hat{V} = \frac{1 - 3\cos^2\theta}{4\pi\epsilon_0 R^3}\hat{d}_{\mathrm{z}}\hat{d}'_{\mathrm{z}}, \tag{S2}$$

where $\hat{d}_{\mathrm{z}}$,$\hat{d}'_{\mathrm{z}}$ are the dipole operator acting on the internal rotational states of the two molecules $\langle N, m_{\mathrm{N}}|\hat{d}_{\mathrm{z}}|N', m_{\mathrm{N}'}\rangle$ respectively. θ is the angle between the direction of relative motion and the polarized dipoles. In this specific case, this coupling describes a process where the rotation is transferred from one molecule to the other.

Identical fermionic molecules like KRb collide dominantly with $L = 1$ in the ultracold regime. We further take the $m_L = 1$ channel for example. The resonant shielding at $\vec{E}_{\mathrm{s}}$ arises from the dipolar coupling between these two channels:

$$\begin{aligned} |\phi_1\rangle &= |L = 1, m_L = 1\rangle|1, 0\rangle|1, 0\rangle \\ |\phi_2\rangle &= |L = 1, m_L = 1\rangle|0, 0\rangle|2, 0\rangle, \end{aligned} \tag{S3}$$

To keep the notations light, we used $|0, 0\rangle|2, 0\rangle$ as a short-hand notation for the properly symmetrized wavefunction $1/\sqrt{2}(|0, 0\rangle|2, 0\rangle + |2, 0\rangle|0, 0\rangle)$ of the properly dressed states in

the electric field. The effects of the dipolar coupling can be shown by writing down the system's Hamiltonian in the basis $|\phi_1\rangle, |\phi_2\rangle$. The diagonal terms, which are the energy of each channel in the absence of the dipolar coupling, read

$$\begin{aligned} E_1(R) &= \langle\phi_1|\hat{H}|\phi_1\rangle = -\frac{C_6}{R^6} + \Theta(R)d_1^2 + \frac{C_2}{R^2} + \Delta_1(\epsilon) \\ E_2(R) &= \langle\phi_2|\hat{H}|\phi_2\rangle = -\frac{C_6}{R^6} + \Theta(R)(d_0 d_2 + d_{02}^2) + \frac{C_2}{R^2} + \Delta_2(\epsilon) \end{aligned} \tag{S4}$$

where

$$\Theta(R) = \langle L = 1, m_L = 1|\frac{1 - 3\cos^2\theta}{4\pi\epsilon_0 R^3}|L = 1, m_L = 1\rangle.$$

The C_6/R^6 is the Van der Waals term which arises from the dipolar coupling between these two states and all the other possible collisional states out of this Hilbert space. These states are far-detuned from either $|\phi_1\rangle$ or $|\phi_2\rangle$. As a result, their contributions reduce to a potential energy term proportional to $1/R^6$ as a second-order perturbation. We use the same C_6 for $|\phi_1\rangle$ and $|\phi_2\rangle$. This is justified by the fact that the dominant contributions to the C_6 is from the couplings to the electronic excited states of the molecules which are independent of the molecular rotation [3]. The C_2/R^2 term is the centrifugal potential where $C_2 = L(L+1)\hbar^2/m$, which is the same for both the channels. The $\propto 1/R^3$ term describes the *direct* dipolar interaction between the two colliders with induced dipole moments of $d_1 = \langle 1, 0|\hat{d}_z|1, 0\rangle, d_0 = \langle 0, 0|\hat{d}_z|0, 0\rangle, d_2 = \langle 2, 0|\hat{d}_z|2, 0\rangle$,$d_{02} = \langle 0, 0|\hat{d}_z|2, 0\rangle$ [4]. This term corresponds to the classical dipole-dipole interactions. The last term is the DC Stark shift in an electric field ϵ. By varying the strength of ϵ, the relative energy between the two channels can be changed.

The coupling between the two channels arising from the dipolar interaction can be written as

$$\Omega(R) = \langle\phi_1|\hat{V}|\phi_2\rangle = \Theta(R)d_{01}d_{12}. \tag{S5}$$

Here $d_{01} = \langle 0, 0|\hat{d}_z|1, 0\rangle, d_{12} = \langle 1, 0|\hat{d}_z|2, 0\rangle$.

The full Hamiltonian including the dipolar coupling in this basis $\{|\phi_1\rangle, |\phi_2\rangle\}$ is then simplified to be

$$H_{m_L=+1}(R) = \begin{bmatrix} E_1(R) & \Omega(R) \\ \Omega(R) & E_2(R) \end{bmatrix} \tag{S6}$$

The effective intermolecular potential that molecules experience at R is the eigenvalue of $H_{m_L=+1}(R)$ at that position, which does not necessarily agree with $E_1(R)$ or $E_2(R)$ when

the off-diagonal coupling presents. A standard avoided-crossing picture suggests that the energy of one channel is pushed up, effectively as a repulsive potential, while the energy of the other is pushed down, effectively as an attractive potential. Depending on the detuning between the two channels, the effective potential can be either repulsive or attractive for each of the channels. The strength of the coupling is proportional to $1/R^3$, therefore the closer the two molecules get, the stronger this effect is. For the channel experiencing an effective repulsion, this R dependence effectively leads to an repulsive barrier.

The detuning between the two channels $\delta(R) = E_2(R) - E_1(R)$ depends on R and can be tuned by ϵ. The resonant field strength ϵ is defined as the field at which $\Delta_1(\epsilon) = \Delta_2(\epsilon)$. For the two channels considered in this work for KRb, the resonant field sits around 12.6 kV/cm. At a slightly higher field, $|1,0\rangle|1,0\rangle$ has higher energy, and the dipolar coupling creates a repulsive barrier on this channel. The barrier suppresses the two-body loss, as in the case of 12.72 kV/cm in this work. At a lower field, the effective potential is attractive, as for 12.50 kV/cm, enhancing the loss.

Fig. S1 displays $E_1(R), E_2(R)$ and the effective potentials with the coupling for different ϵ. The potential zero reference is chosen such that $E_1(R) \to 0$ at infinity. We use realistic parameters for KRb at 12.72 kV/cm: $C_6 = 12636\ E_\mathrm{h} a_0^6$ [3] with E_h being the Hartree energy, $d_0 = 0.33$ D, $d_2 = -0.1$ D, $d_1 = -0.08$ D, $d_{01} = 0.2$ D, $d_{12} = 0.29$ D, $d_{02} = -0.06$ D. We simply assume that $\Omega(R) = 1/(4\pi\epsilon_0)R^3$, which would not change the picture qualitatively. Fig. S1 shows a potential barrier height of $\sim 550\ \mu$K for the parameter chosen.

The simplified Hamiltonian Eq. S6 immediately reveals several features of the shielding mechanism. The height of the barrier is expected to be on the order of $\Omega(R_0)$ where $R_0 \sim 170 a_0$ is the intermolecular separation the two channels become degenerate. The height is therefore $V \sim \Omega(R_0) \approx 700\ \mu$K. The width of the shielding resonance W_E can be estimated by calculating the range of ϵ over which $\Delta_1 - \Delta_2$ changed by $\Omega(R_0)$

$$W_\mathrm{E} \sim \frac{\Omega(R_0)}{|(d_2 + d_0 - 2d_1)|} \approx 166\ \mathrm{V/cm}, \tag{S7}$$

which depends on the differential dipole between the two channels.

Similarly, we can calculate the effective potential for the $|L = 1, m_L = 0\rangle$ collisions. It can also be translated directly to calculate the effect between collisional channels that are coupled with similar mechanism such the $|1,0\rangle|1,0\rangle \to |0,0\rangle|2,\pm 1\rangle$, though for this case the coupling requires a transfer of angular momentum between the orbits and the internal

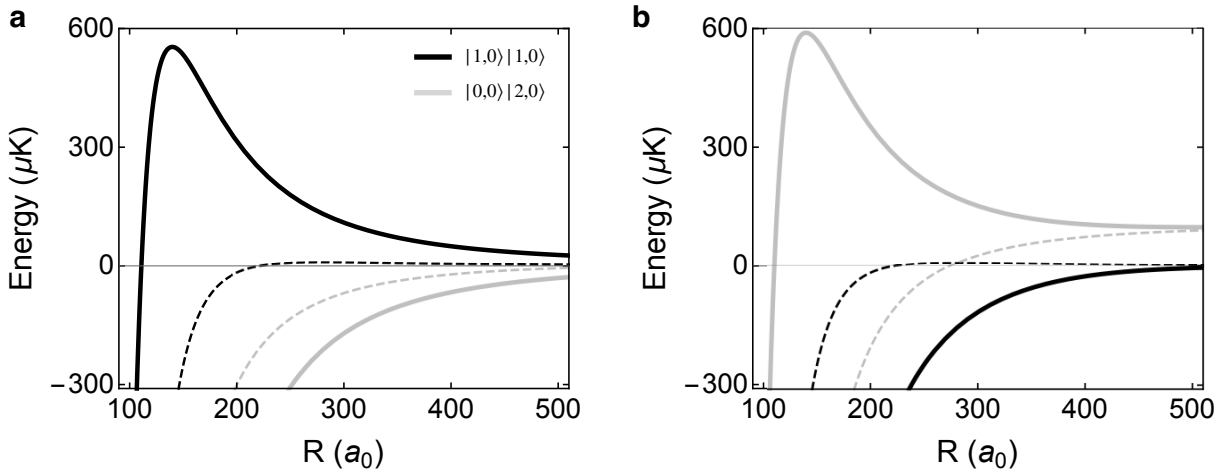

FIG. S1. **Effective intermolecular potentials with the resonant dipolar coupling.** Black and gray curves are the potential for $|1,0\rangle|1,0\rangle$ and $|0,0\rangle|2,0\rangle$ respectively. Solid and dashed lines are the potential with and without the resonant dipolar coupling. **a**, When internal energy of the $\Delta_2 < \Delta_1$, resonant dipolar coupling creates an energy barrier on channel $|1,0\rangle|1,0\rangle$ due to the avoided crossing. This is the scenario for $|\boldsymbol{E}| = 12.72$ kV/cm. **b**, When $\Delta_2 > \Delta_1$ has higher energy, the potential for the $|1,0\rangle|1,0\rangle$ channel is pushed down, enhancing the loss.

rotation which is not explicitly written in Eq. S2.

Though the height and the width of the resonance may vary quantitatively between different species of molecules, the qualitative derivation we demonstrate here is valid for fermionic molecules. This highlights the generality of the shielding mechanism.

The resonant shielding effect is fundamentally different from the rate suppression due to the classical dipolar repulsion [5, 6], which is captured by the diagonal terms in Eq. S6. While the classical repulsion from the direct dipolar interaction creates a barrier for the "side-to-side" collisions, it exerts an attractive interaction for the "head-to-tail" collisions [7]. In contrast, in the resonant regime, the barrier exists for both types of the collisions, enabling 3D shielding of the two-body loss.

Figure S1 provide semi-quantitative values of the effective intermolecular potentials of the colliding system after averaging over the incident partial wave and the orbital angles. This is convenient to understand the overall picture of the collision in term of the radial motion only. To get more insights on the anisotropic angular aspect of the shielding mechanism in three dimensions and before averaging over the partial waves, one can also plot the dipolar

potential energy which contains explicitly the dependence on θ. In that way, the angular dependence is kept and illustrates the anisotropic collisional shielding at the microscopic level. We can then define two potential energy surfaces [8] coming from the diagonalization of a two-by-two matrix with energies

$$\frac{d_1^2\,(1-3\cos^2\theta)}{4\pi\varepsilon_0\,R^3}+\Delta_1(\epsilon) \tag{S8}$$

$$\frac{(d_0\,d_2+d_{02}^2)\,(1-3\cos^2\theta)}{4\pi\varepsilon_0\,R^3}+\Delta_2(\epsilon) \tag{S9}$$

and a coupling

$$\sqrt{2}\,\frac{d_{10}\,d_{12}\,(1-3\cos^2\theta)}{4\pi\varepsilon_0\,R^3}. \tag{S10}$$

For a given (R,θ), if Eq. (S8) $\geq$ Eq. (S9), we define

$$V_{\pm}(R,\theta)=\frac{1}{2}\left(\frac{(d_1^2+d_0\,d_2+d_{02}^2)\,(1-3\cos^2\theta)}{4\pi\varepsilon_0\,R^3}+\Delta_1(\epsilon)+\Delta_2(\epsilon)\right)$$
$$\pm\frac{1}{2}\sqrt{\left(\frac{(d_1^2-d_0\,d_2-d_{02}^2)\,(1-3\cos^2\theta)}{4\pi\varepsilon_0\,R^3}+\Delta_1(\epsilon)-\Delta_2(\epsilon)\right)^2+4\left(\sqrt{2}\,\frac{d_{10}\,d_{12}\,(1-3\cos^2\theta)}{4\pi\varepsilon_0\,R^3}\right)^2}. \tag{S11}$$

If Eq. (S8) $<$ Eq. (S9), we similarly define

$$V_{\pm}(R,\theta)=\frac{1}{2}\left(\frac{(d_1^2+d_0\,d_2+d_{02}^2)\,(1-3\cos^2\theta)}{4\pi\varepsilon_0\,R^3}+\Delta_1(\epsilon)+\Delta_2(\epsilon)\right)$$
$$\pm\frac{1}{2}\sqrt{\left(\frac{(d_0\,d_2+d_{02}^2-d_1^2)\,(1-3\cos^2\theta)}{4\pi\varepsilon_0\,R^3}+\Delta_2(\epsilon)-\Delta_1(\epsilon)\right)^2+4\left(\sqrt{2}\,\frac{d_{10}\,d_{12}\,(1-3\cos^2\theta)}{4\pi\varepsilon_0\,R^3}\right)^2}. \tag{S12}$$

When $\Delta_1(\epsilon)>\Delta_2(\epsilon)$, the $V_+(R,\theta)$ surface is the one that correlates to the initial state $|1,0\rangle\,|1,0\rangle$ at large distance. This is the case for $\epsilon=12.72$ kV/cm and we plotted in Fig. 1**b** the surface

$$V_+(R,\theta)-\frac{C_6}{R^6}+\frac{C_2}{R^2} \tag{S13}$$

to also account for the van der Waals interaction and the centrifugal barrier. When $\Delta_1(\epsilon)<\Delta_2(\epsilon)$, the $V_-(R,\theta)$ surface is now the one that correlates to the initial state $|1,0\rangle\,|1,0\rangle$. This is the case for $\epsilon=12.5$ kV/cm and we plotted in Fig. 1**a** the surface

$$V_-(R,\theta)-\frac{C_6}{R^6}+\frac{C_2}{R^2}. \tag{S14}$$

THERMALIZATION IN DIPOLAR GASES OF FERMIONS

A dipolar gas out of thermal equilibrium comes back to equilibrium by means of collisions, at a rate proportional to the mean elastic cross section, $\sigma_{\rm el}$ [9–12]. However, dipolar anisotropies can cause the effectiveness of each collision for rethermalization to vary. This manifests in a dipole-alignment dependence of "the number of collisions required per particle for thermalization", $N_{\rm coll}$ – a collective measure for the redistribution of energy through a gas via elastic collisions [12–14].

We derive the quantity $N_{\rm coll}$ in the close-to-equilibrium limit, through a method of averages approach. We envision a Gaussian distributed phase space ensemble in all coordinates, but initialized with a slightly greater width in the y direction as in the experiment to simulate parametric excitation. We then track the Gaussian width in the x direction by having rethermalization observed over time in the energy differential

$$\langle\chi\rangle \equiv E_{\rm x} - k_{\rm B}T_{\rm eq}, \tag{S15}$$

where $T_{\rm eq}$ is the equilibration temperature (obtainable from the equipartition theorem), $\langle\ldots\rangle$ denotes a thermal average assuming Gaussian phase space distribution, and $E_{\rm x} = \frac{\langle p_{\rm x}^2\rangle}{2m} + \frac{1}{2}m\omega_{\rm x}^2\langle x^2\rangle$ is the sum of kinetic and potential energy in the x-direction. The Enskog equations in Ref. [15] dictate that the relaxation of $\langle\chi\rangle$ follows the differential equation

$$\frac{d\langle\chi\rangle}{dt} = \mathcal{C}_F[\chi] = \left(\frac{4N}{315\pi}\right)\left(\frac{a_d^2 m^2\overline{\omega}^3}{k_{\rm B}T_0}\right)\big[4\left(\langle p_{\rm x}^2\rangle - \langle p_{\rm z}^2\rangle\right)\cos(2\theta) + 17\left(\langle p_{\rm x}^2\rangle - \langle p_{\rm y}^2\rangle\right)\cos(4\theta) - 45\langle p_{\rm x}^2\rangle + 33\langle p_{\rm y}^2\rangle + 12\langle p_{\rm z}^2\rangle\big], \tag{S16}$$

where N is the number of molecules, m is the molecular mass, $\overline{\omega}$ is the geometric mean of trapping frequencies and $k_{\rm B}T_0$ is the pre-excitation thermal energy. The analytic collision integral $\mathcal{C}_F$, is calculated using the techniques developed in Ref. [15], but using the differential cross sections for fermions as described in Ref. [13]. For small deviations from equilibrium and at short times, this can be approximated with a decay rate γ, as $\mathcal{C}[\chi] \approx -\gamma\langle\chi\rangle$, which results in the relation

$$\gamma = -\frac{1}{(E_{\rm x} - k_{\rm B}T_{\rm eq})}\frac{dE_{\rm x}}{dt}. \tag{S17}$$

With $N_{\rm coll} = n\sigma_{\rm el}v/\gamma$, we arrive at the simple expression:

$$N_{\rm coll}(\theta) = \frac{56}{33 - 17\cos(4\theta)}. \tag{S18}$$

A more comprehensive discussion of these rethermalization measures for elastic dipoles is left to an upcoming publication.

[1] G. Wang and G. Quéméner, New Journal of Physics **17**, 035015 (2015).

[2] A. V. Avdeenkov, M. Kajita, and J. L. Bohn, Phys. Rev. A **73**, 022707 (2006).

[3] M. Lepers, R. Vexiau, M. Aymar, N. Bouloufa-Maafa, and O. Dulieu, Phys. Rev. A **88**, 032709 (2013).

[4] A. V. Gorshkov, S. R. Manmana, G. Chen, E. Demler, M. D. Lukin, and A. M. Rey, Phys. Rev. A **84**, 033619 (2011).

[5] G. Valtolina, K. Matsuda, W. G. Tobias, J.-R. Li, L. De Marco, and J. Ye, Nature **588**, 239 (2020).

[6] M. H. G. de Miranda, A. Chotia, B. Neyenhuis, D. Wang, G. Quéméner, S. Ospelkaus, J. L. Bohn, J. Ye, and D. S. Jin, Nature Physics **7**, 502 (2011).

[7] K. K. Ni, S. Ospelkaus, D. Wang, G. Quéméner, B. Neyenhuis, M. H. G. de Miranda, J. L. Bohn, J. Ye, and D. S. Jin, Nature **464**, 1324 (2010).

[8] Lassablière et. al., in preparation.

[9] C. R. Monroe, E. A. Cornell, C. A. Sackett, C. J. Myatt, and C. E. Wieman, Phys. Rev. Lett. **70**, 414 (1993).

[10] P. O. Schmidt, S. Hensler, J. Werner, A. Griesmaier, A. Görlitz, T. Pfau, and A. Simoni, Phys. Rev. Lett. **91**, 193201 (2003).

[11] N. R. Newbury, C. J. Myatt, and C. E. Wieman, Phys. Rev. A **51**, R2680 (1995).

[12] Y. Tang, A. Sykes, N. Q. Burdick, J. L. Bohn, and B. L. Lev, Phys. Rev. A **92**, 022703 (2015).

[13] J. L. Bohn and D. S. Jin, Phys. Rev. A **89**, 022702 (2014).

[14] A. G. Sykes and J. L. Bohn, Phys. Rev. A **91**, 013625 (2015).

[15] R. R. W. Wang, A. G. Sykes, and J. L. Bohn, Phys. Rev. A **102**, 033336 (2020).